

Metal–Organic Frameworks

Analysis of High and Selective Uptake of CO₂ in an Oxamide-Containing {Cu₂(OOCR)₄}-Based Metal–Organic Framework

Nada H. Alsmail, Mikhail Suyetin, Yong Yan, Rafel Cabot, Cristina P. Krap, Jian Lü, Timothy L. Easun, Elena Bichoutskaia, William Lewis, Alexander J. Blake, and Martin Schröder^{*[a]}

Abstract: The porous framework [Cu₂(H₂O)₂L]·4H₂O·2DMA (H₄L = oxalylbis(azanediyl)diisophthalic acid; DMA = *N,N*-dimethylacetamide), denoted NOTT-125, is formed by connection of {Cu₂(RCOO)₄} paddlewheels with the isophthalate linkers in L⁴⁻. A single crystal structure determination reveals that NOTT-125 crystallises in monoclinic unit cell with $a = 27.9161(6)$, $b = 18.6627(4)$ and $c = 32.3643(8)$ Å, $\beta = 112.655(3)^\circ$, space group $P2_1/c$. The structure of this material shows **fof** topology, which can be viewed as the packing of two types of cages (cage A and cage B) in three-dimensional space. Cage A is constructed from twelve {Cu₂(OOCR)₄} paddlewheels and six linkers to form an ellipsoid-shaped cavity approximately 24.0 Å along its long axis and 9.6 Å across its central diameter. Cage B consists of six {Cu₂-

(OOCR)₄} units and twelve linkers and has a spherical diameter of 12.7 Å taking into account the van der Waals radii of the atoms. NOTT-125 incorporates oxamide functionality within the pore walls, and this, combined with high porosity in desolvated NOTT-125a, is responsible for excellent CO₂ uptake (40.1 wt% at 273 K and 1 bar) and selectivity for CO₂ over CH₄ or N₂. Grand canonical Monte Carlo (GCMC) simulations show excellent agreement with the experimental gas isotherm data, and a computational study of the specific interactions and binding energies of both CO₂ and CH₄ with the linkers in NOTT-125 reveals a set of strong interactions between CO₂ and the oxamide motif that are not possible with a single amide.

Introduction

Metal–organic frameworks (MOFs) show great promise for applications in gas storage and separation because these crystalline, porous materials can demonstrate exceptionally high internal surface areas and tunable functional pore environments.^[1] Notably, CO₂ storage in MOFs^[2] compares extremely favourably with other classes of porous materials, such as zeolites, activated carbon and silica.^[3] Great efforts have been focused on enhancing the binding affinity and selectivity of MOFs towards CO₂, and several strategies have been reported to enhance gas storage.^[4] The shape, size and chemical environment of the pores within a MOF play significant roles in gas storage capacity, specificity and separations.^[1d,5] The physical characteristics of pore volume and surface area have been shown to correlate strongly with the high pressure (> 20 bar) CO₂ uptake in MOFs, with physisorption dominating, while the strength of gas–framework interactions correlates strongly with the low pressure (< 1 bar) CO₂ uptake of a framework.^[6]

The primary approaches to controlling the chemical characteristics of the pores and hence the strength of the gas–framework interaction are by modification of the ligands either by incorporating functional groups prior to the formation of MOFs or by post-synthetic modification in which functional groups such as –NH₂, –OH or –CHO moieties are generated within the frameworks.^[3c,6–10] Nitrogen-containing groups or open metal sites accessible within the pores can improve CO₂ affinity via dipole–quadrupole interactions with the CO₂ molecules.^[11–14] We recently described the material NOTT-122 incorporating triazole groups, which displays a high adsorption capacity for CO₂, and used a computational approach to investigate the specific interactions between CO₂ and the framework linker heteroatoms.^[15] Similarly, Zaworotko et al. have reported MOFs^[16] containing amide functional groups in the linkers, whereby linking of three isophthalates generated polyhedral structures that exhibit a strong binding affinity for CO₂.^[16–18]

Our general approach has been based on the use of highly symmetric polydentate carboxylate ligands to construct porous coordination polymers, which demonstrate excellent gas uptake and selectivity.^[19–21] We describe herein the synthesis and gas uptake properties of NOTT-125, an amide-containing MOF primarily distinguished by the “double amide” [–NHC(O)C(O)NH–] oxamide motif within the bridging ligand L⁴⁻ (H₄L = oxalylbis(azanediyl)diisophthalic acid) whereby two back-to-back amides comprise the bridge between two isophthalate groups. This linker connects {Cu₂(OOCR)₄} paddle-

[a] N. H. Alsmail, Dr. M. Suyetin, Dr. Y. Yan, Dr. R. Cabot, Dr. C. P. Krap, Dr. J. Lü, Dr. T. L. Easun, Prof. Dr. E. Bichoutskaia, Dr. W. Lewis, Prof. Dr. A. J. Blake, Prof. Dr. M. Schröder

School of Chemistry, University of Nottingham
Nottingham NG7 2RD (UK)

E-mail: m.schroeder@nottingham.ac.uk

Supporting information for this article is available on the WWW under <http://dx.doi.org/10.1002/chem.201304005>.

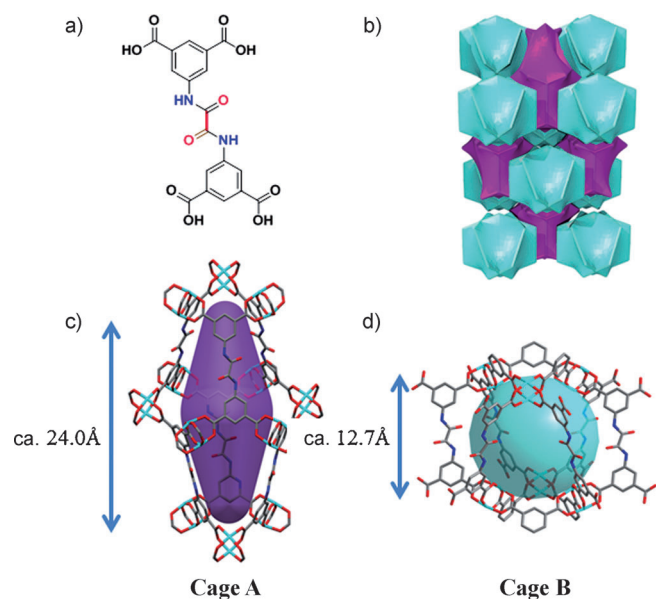
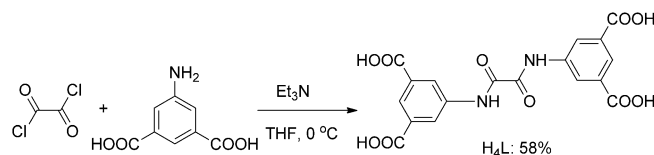


Figure 1. View of: a) chemical structure of H₄L; b) tiling of NOTT-125; c) cage A, and d) cage B.

wheels to form a MOF of **fof** topology in which the oxamide is incorporated and placed within the pore walls (Figure 1). NOTT-125 exhibits a high surface area and excellent CO₂ uptake (40.1% at 1 bar, 273 K). To the best of our knowledge NOTT-125 displays the third highest reported CO₂ uptake in a MOF and shows significant selectivity for CO₂ versus both N₂ and CH₄ (Table 1). Importantly, grand canonical Monte Carlo (GCMC) simulations of the isotherms show excellent agreement with the experimental data, and a computational study into the specific interactions and binding energies of both CO₂ and CH₄ with the linkers reveals a set of strong interactions between CO₂ and the oxamide motif, which are not possible with only a single amide. As far as we are aware, this is the first time that the oxamide motif has been employed within a MOF design.

Results and Discussion

H₄L was synthesised in high yield by treatment of oxalyl chloride and 5-aminoisophthalic acid in tetrahydrofuran (THF; Scheme 1). The solvothermal reaction of H₄L and Cu-



Scheme 1. Synthesis of H₄L.

(NO₃)₂·3H₂O in *N,N*-dimethylacetamide (DMA)/water (6:1) under acidic (HBF₄) conditions yielded blue crystals of [Cu₂-(H₂O)₂L]-4H₂O·2DMA in 70% yield. We found that DMA is a better solvent than DMF in this reaction and leads to the formation of more crystalline and porous products. The as-synthesised material is insoluble in common organic solvents and was characterised by single-crystal X-ray diffraction, powder X-ray diffraction, elemental analysis and thermogravimetric analysis. A single crystal structure determination revealed that NOTT-125 crystallises in monoclinic cell with $a=27.9161(6)$, $b=18.6627(4)$ and $c=32.3643(8)$ Å, $\beta=122.655(3)^\circ$, space group $P2_1/c$. The three-dimensional porous framework hosts DMA and H₂O solvent molecules. Two Cu^{II} cations are bridged by four carboxylate groups distributed around the Cu–Cu axis to form a {Cu₂(OOCR)₄} paddlewheel node with the structure extended by bridging L⁴⁻ linkers to form a porous 3D structure (Figure S2 in the Supporting Information). The overall structure of NOTT-125 has **fof** topology^[22] which can be viewed as the packing of two types of cages (cage A and B) in three-dimensional space (Figure 1). Cage A is constructed by twelve {Cu₂-(OOCR)₄} paddlewheels and six linkers to form an ellipsoid-shaped cavity approximately 24.0 Å along its long axis and 9.6 Å across the central diameter. Cage B consists of six {Cu₂-(OOCR)₄} units and twelve linkers with a spherical diameter of 12.7 Å taking into account the van der Waals radii of the atoms. It is worth noting that the structure is densely decorated with amide functionalities that are directly exposed in both cages. There are two types of pore window between cage A and B. The smaller window is an equilateral triangle, the vertices of which are occupied by {Cu₂(COO)₄} paddlewheels with a distance of 9.3 Å between their centroids. The larger window takes the shape of an isosceles triangle (13.9×13.9×9.3 Å) constructed by two linkers and one isophthalate unit.

The total accessible volume of NOTT-125 after removal of the guest and coordinated water molecules is estimated to be 71% using the PLATON/VOID routine^[23] and the calculated density of the desolvated framework is 0.672 g cm⁻³. NOTT-125 shows thermal stability up to 280 °C by thermogravimetric analysis (TGA; Figure S3 in the Supporting Information), and the phase purity of the bulk sample was confirmed by powder X-ray diffraction (PXRD; Figure S4 in the Supporting Information). The fully desolvated framework NOTT-125a was prepared by

Material	BET [m ² g ⁻¹]	Pore volume [cm ³ g ⁻¹]	CO ₂ uptake [wt%] at 273 K, 1 bar	CO ₂ uptake [wt%] at 298 K, 1 bar	Q _{st} [kJ mol ⁻¹]	Ref.
NJU-Bai-3	2690	1.08	27.3	10.0	36.5	[26]
[Cu ₃ (TPBTM)]	3160	1.27	42.6	23.28	26.3	[16a]
[Cu ₃ (TDPAT)]	1938	0.93	44.5	25.8	42.2	[25]
PCN-124	1372	0.58	28.6	–	26.3	[24]
[Cu ₃ (BDPT)] HNUST-1	1400	0.57	30.7	18.26	31.2	[26]
NOTT-125	2471	1.1	40.0	18.19	25.4	this work
NOTT-122	3286	1.41	39.7	20.4	24.5	[15]
PCN-61	3350	1.37	21.4	–	22.0	[16b]
PCN-66	4000	1.63	22.1	–	26.2	[16b]
PCN-68	5109	2.13	22.1	–	21.2	[16b]

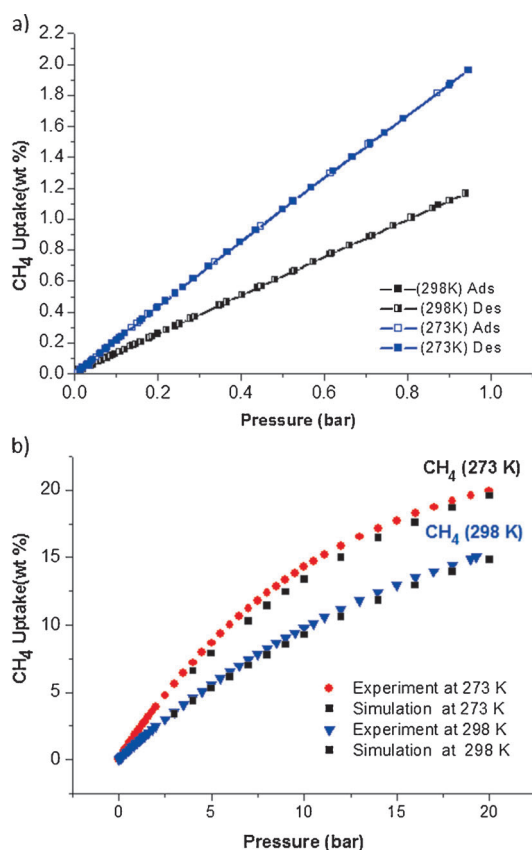


Figure 2. a) Experimental CH₄ isotherms of NOTT-125a at 273 and 298 K in the pressure range 0–1 bar; b) experimental and simulated CH₄ isotherms of NOTT-125a at 273 and 298 K up to 20 bar.

soaking the sample in acetone for five days followed by heating at 100 °C and 10⁻¹⁰ bar for 1 day. PXRD analysis after desolvation indicates that the framework structure of NOTT-125a retains crystallinity and remains intact on activation (Figure S4 in the Supporting Information). All subsequent analyses described below were performed on the activated NOTT-125a.

The permanent porosity of activated NOTT-125a was confirmed by gas adsorption measurements. The N₂ sorption isotherm for NOTT-125a at 77 K exhibits reversible type I adsorption behaviour characteristic of a microporous material (Figure S5 in the Supporting Information). The Brunauer–Emmett–Teller (BET) surface area was measured as 2447 m²g⁻¹ (Figure S6 in the Supporting Information) based upon the N₂ sorption isotherm, and the calculated total pore volume of NOTT-125a is 1.1 cm³g⁻¹. The pore size distribution (PSD) was calculated according to the N₂ isotherm using non-local density functional theory (NLDFT) implementing a hybrid kernel based on a zeolite-silica model containing cylindrical pores. The PSD was found to lie in the range 10–13 Å (Figure S7 in the Supporting Information), consistent with the single crystal structure determination.

The gravimetric CH₄ sorption isotherms for NOTT-125a were recorded up to 1 bar at 273 and 298 K, with both isotherms showing good reversibility and a moderate total uptake of CH₄ of 2.10 wt% (1.31 mmol g⁻¹) and 1.34 wt% (0.837 mmol g⁻¹),

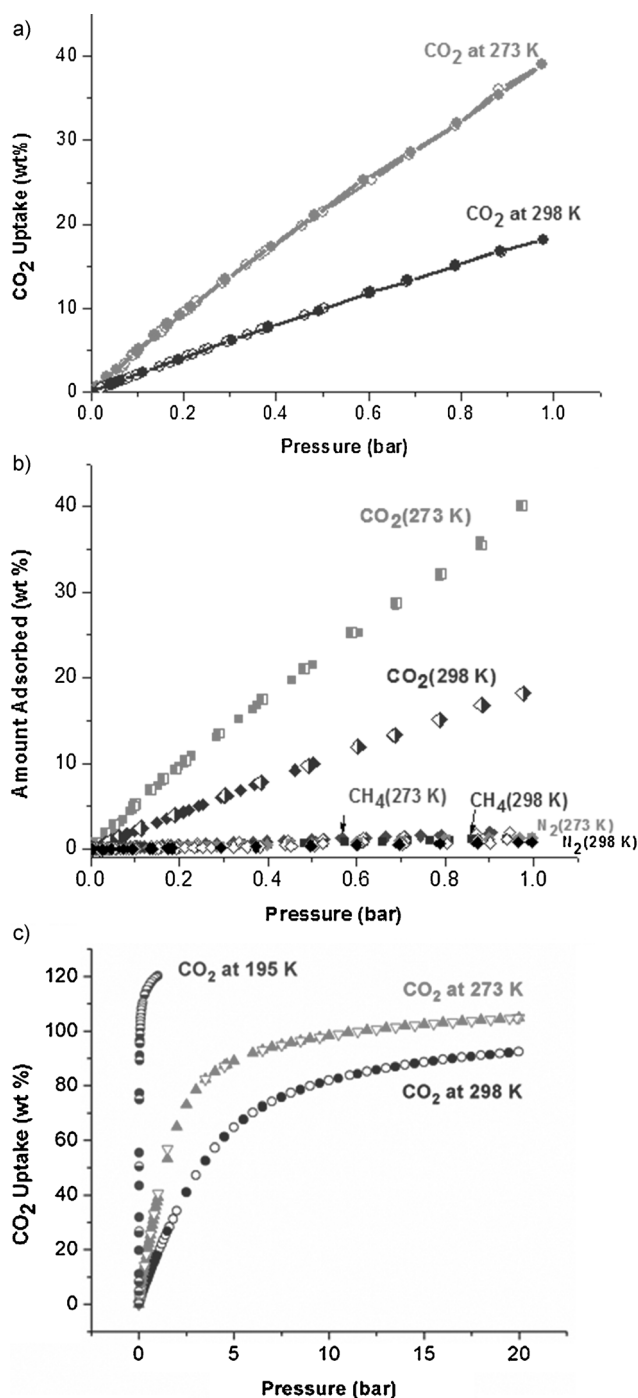


Figure 3. a) CO₂ sorption isotherms of NOTT-125a at 273 and 298 K up to 1 bar; b) CO₂, CH₄ and N₂ sorption isotherms for NOTT-125a at 273 and 298 K up to 1 bar and c) CO₂ sorption isotherms of NOTT-125a at 195, 273 and 298 K up to 20 bar.

respectively. By comparison, the related amide-containing PCN-124 framework described by Zhou et al. shows CH₄ uptake of 2.33 wt% at 273 K.^[24] At 20 bar NOTT-125 shows a CH₄ uptake of 20.4 wt% (192 cm³cm⁻³ at standard temperature and pressure (STP)) at 273 K and 15.1 wt% (142.1 cm³cm⁻³) at 298 K (Figure 2). The isosteric heat of CH₄ adsorption was found by virial analysis to be 14.5 kJ mol⁻¹ at zero surface coverage (Figure S10 in the Supporting Information).

Combined with the large pore volume, the oxamide groups in the pore walls were expected to enhance uptake of CO₂ in the framework and indeed this is evident in the low pressure (up to 1 bar) isotherms recorded at 273 and 298 K. Both isotherms are completely reversible and show no hysteresis. At 273 K, the total uptake reaches 40.1 wt% (9.09 mmol g⁻¹, 203.7 cm³ g⁻¹; Figure 3). At 298 K the total uptake is 18.19 wt% (4.13 mmol g⁻¹, 92.59 cm³ g⁻¹; Figure 3). The total CO₂ uptake approaches the highest reported values for MOFs, such as Cu-TDPAT^[25] (44.5 wt%, 273 K, 1 bar) and Cu-TPBTM^[16a] (42.6 wt%, 273 K, 1 bar), and a comparison with a range of relevant MOFs is presented in Table 1. Significantly, in comparison with the related amide-functionalised MOF Cu-NJU-Bai3,^[26] NOTT-125a shows higher CO₂ uptake at 1 bar (NJU-Bai3: 27.3 wt%, 6.21 mmol g⁻¹, 273 K) and also higher uptake under the same conditions than the amide functionalised MOF PCN-124^[24] (28.6 wt%, 6.5 mmol g⁻¹, 273 K). NOTT-125a also shows a high CO₂ uptake of 21.2 mmol g⁻¹ at 298 K and 20 bar (Figure 4).

The excellent uptake of CO₂ observed in the low pressure isotherms is consistent with the presence of specific CO₂-amide interactions. There are several potential interactions that

can be proposed including dipole-quadrupole interactions of the type described above^[11-14] and hydrogen-bond formation between the amide NH and the oxygen atoms of CO₂.^[16] To better understand these observations, the isosteric heat (Q_{st}) of adsorption of CO₂ was calculated by fitting the CO₂ sorption isotherms at 273 and 298 K to a virial-type equation. The isosteric heat is estimated to be 25.35 kJ mol⁻¹ at zero surface coverage.

The marked difference in CH₄ and CO₂ adsorption isotherms encouraged us to examine the capability of NOTT-125a for selective capture of CO₂ versus N₂ and CO₂ versus CH₄. To evaluate the selective CO₂ capture in NOTT-125a, CH₄ and N₂ sorption isotherms were measured at 273 and 298 K (Figure 3b) up to 1 bar. By determining the ratios of the Henry's law constants from single component isotherms,^[27] the CO₂/N₂ adsorption selectivity factors for NOTT-125a are 20.7:1 at 273 K and 16:1 at 298 K, further suggesting that the polar amide functionalities have a positive effect on CO₂ adsorption. Furthermore, NOTT-125a also shows respectable CO₂/CH₄ selectivity of 9.2:1 at 273 K and 4.8:1 at 298 K.

Gravimetric H₂ sorption measurements performed on NOTT-125a at 77 and 87 K up to 1 bar show completely reversible isotherms with an absence of hysteresis and moderate H₂ storage capacity of 2.30 and 1.48%, respectively (Figure 5). The iso-

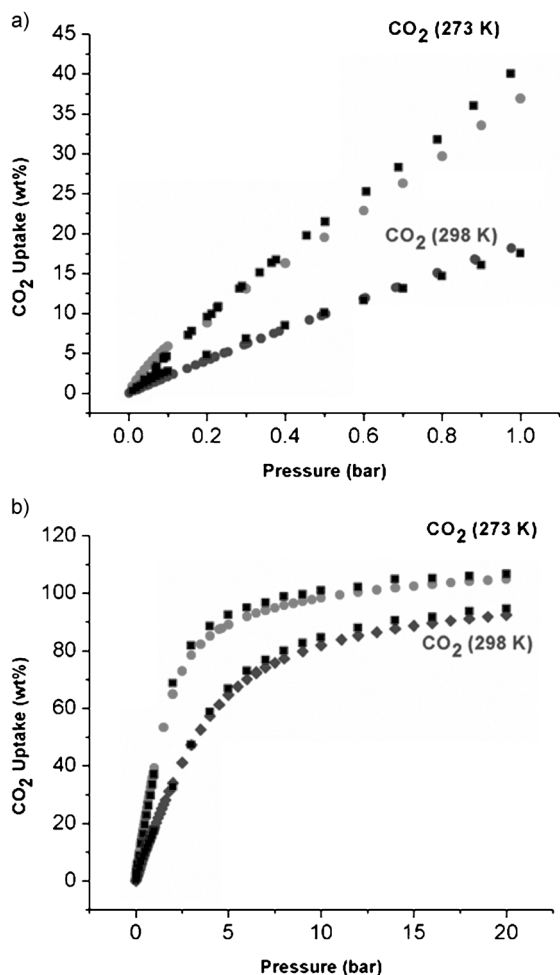


Figure 4. a) Experimental (circles) and simulated (squares) CO₂ isotherms of NOTT-125a at 273 and 298 K in the pressure range 0–1 bar; b) experimental (circles) and simulated (squares) CO₂ isotherms of NOTT-125a at 273 and 298 K up to 20 bar.

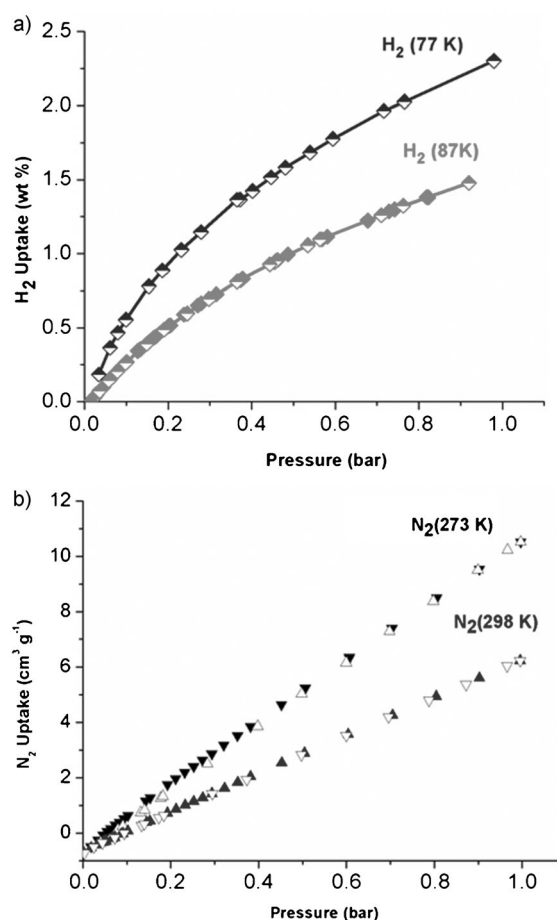


Figure 5. a) H₂ isotherms of NOTT-125a at 77 and 87 K up to 1 bar; b) N₂ isotherms of NOTT-125a at 273 and 298 K up to 1 bar.

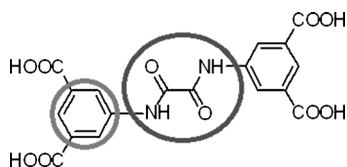


Figure 6. Two adsorption sites for CO₂ on the NOTT-125a linker examined by the calculations: the oxamide part and phenyl ring are highlighted by circles.

steric heat of adsorption (Q_{st}) for H₂ was found to be 5.1 kJ mol⁻¹ at zero surface coverage.

Grand canonical Monte Carlo (GCMC) calculations were performed to simulate the adsorption of both CO₂ and CH₄ in NOTT-125a. Figures 2 and 4 show simulated isotherms for CH₄ and CO₂ uptake, respectively, in NOTT-125a, and these are in excellent agreement with the experimentally measured isotherms. To understand further the relevant adsorption mechanisms of the CH₄ and CO₂ molecules to the linkers of NOTT-125a at a molecular level, second order Møller–Plesset perturbation theory (MP2) as implemented in the Q-Chem quantum chemistry package^[28] was employed. We analysed the strength of two preferential adsorption sites in the linker: one formed by two amide –CONH– groups and the other being the phenyl ring (both highlighted in Figure 6). We calculated the binding energies (BE) between the guest molecule and the linker as well as their relative positions corresponding to the strongest binding. For the interactions of CH₄ and CO₂ with the oxamide part of the linker, the calculations were performed in two-stages in each case. For CH₄, the geometry optimisation was carried out using DFT calculations at the B3LYP/6-31G** level of theory and the binding energies were subsequently calculated at the higher B3LYP/6-311++G** level with $BE = E_{opt}(\text{complex}) - E_{opt}(\text{linker}) - E_{opt}(\text{guest molecule})$. For CO₂, the geometry optimisation was first performed at the MP2/cc-pvdz level of theory and the binding energies were subsequently calculated at the higher MP2/cc-pvqz level. Binding energies were corrected for basis set superposition error (BSSE), and the stable configuration identified for the CH₄ molecule and linker is shown in Figure 7. The distance between H(CH₄) and O(amide) is less than the sum of their van der Waals radii, with the binding energy $E = -5.57$ kJ mol⁻¹ characterised by a hydrogen-bond-like interaction, C(CH₄)–H(CH₄)...O(amide), with a C–H...O angle of 178.85°.

We performed an extensive search for CO₂ binding sites and several configurations showing the strongest binding are summarised in Table 2 and Table 3. The strongest binding of CO₂ to the linker was found to be in complexes A and B in which the guest CO₂ molecule interacts with the linker in a side-on fashion and having binding energies of –19.7 and

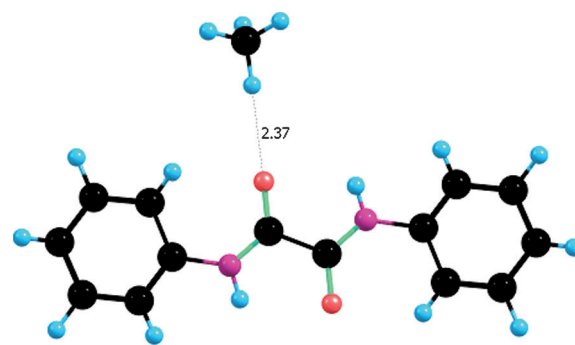


Figure 7. The optimised geometry of the C₁₄H₁₂N₂O₂–CH₄ complex.

Table 2. The optimised MP2/cc-pvdz geometries and MP2/cc-pvqz binding energies of C₁₄H₁₂N₂O₂–CO₂ complexes.

	Optimised geometry	Binding energy [kJ mol ⁻¹]
A		–19.66
B		–16.17
C		–14.92
D		–13.04
E		–12.67
F		–10.25
G		–7.61

Table 3. The structural details of the optimised configurations of $C_{14}H_{12}N_2O_2-CO_2$ complexes corresponding to the strongest binding energies as predicted by the MP2/cc-pvqz level of theory.

Complex	Type of interaction	Distance [Å]	Angle [°]	O=C=O angle [°]
A	H-bond, N-H...O(CO ₂)	2.30, H...O(CO ₂)	164.59, N-H...O(CO ₂)	177.80
	weak H-bond, C-H...O(CO ₂)	2.67, H...O(CO ₂)	142.93, C-H...O(CO ₂)	
	CO...C(CO ₂)	2.78, O...C(CO ₂)	150.00, C-O...O(CO ₂)	
B	H-bond N-H...O(CO ₂)	3.05, NH...O(CO ₂)	175.29, N-H...O(CO ₂)	177.88
	weak H-bond, C-H...O(CO ₂)	2.74, H...O(CO ₂)	164.87, C-H...O(CO ₂)	
	C-O...C(CO ₂)	2.74, O...C(CO ₂)	173.79, C-O...O(CO ₂)	
C	H-bond, N-H...O ₁ (CO ₂)	2.46, H...O ₁ (CO ₂)	129.69, N-H...O ₁ (CO ₂)	178.59
	H-bond, N-H...O ₂ (CO ₂)	3.49, H...O ₂ (CO ₂)	102.26, N-H...O ₂ (CO ₂)	
	weak H-bond, C-H...O ₁ (CO ₂)	2.82, H...O ₁ (CO ₂)	125.42, C-H...O ₁ (CO ₂)	
	C-O...C(CO ₂)	2.91, O...C(CO ₂)	106.17, C-O...O(CO ₂)	
D	C-H...O(CO ₂)	2.8, H...O(CO ₂)	44.7, C-H...O(CO ₂)	178.82
	C-O...C(CO ₂)	2.97, CO...C(CO ₂)	74.01, C-O...C(CO ₂)	
E	C-O...C(CO ₂)	2.93, O...C(CO ₂)	92.17, CO...C(CO ₂)	178.56
	O-C...O(CO ₂)	2.90, C...O(CO ₂)	86.93, OC...O(CO ₂)	
F	C-N...C(CO ₂)	3.02, N...C(CO ₂)	98.82, C-N...C(CO ₂)	179.75
	N-H...O(CO ₂)	2.98, H...O(CO ₂)	98.32, N-H...O(CO ₂)	
G	O-C ₁ ...O(CO ₂)	2.94, C ₁ ...O(CO ₂)	95.57, O-C ₁ ...O(CO ₂)	179.87
	O-C ₂ ...O(CO ₂)	2.91, C ₂ ...O(CO ₂)	97.98, O-C ₂ ...O(CO ₂)	

–16.2 kJ mol⁻¹, respectively. In complex A the interaction is dominated by a strong hydrogen bond (2.30 Å) formed between the electronegative oxygen of CO₂ and the hydrogen of the amide group. This interaction is further enhanced by both the electrostatic attraction between the carbon of CO₂ and the electronegative oxygen of the linker, and a weak C–O...H–C (aromatic) interaction, which can be regarded as a weak hydrogen bond.^[29] All these interactions have a significant cooperative effect on the overall binding of CO₂ to this polyamide core. Complex B corresponds to an in-plane T-shaped orientation of CO₂ and the C–O bond of one of the amide groups of the linker. The electrostatic interaction between carbon of CO₂ and oxygen in the linker is somewhat stronger in this configuration compared to complex A. Complex C (BE = –14.92 kJ mol⁻¹) is stabilised by two hydrogen bonds N–H...O₁(CO₂) and N–H...O₂(CO₂), thus having one donor and two acceptors. The N–H...O₁(CO₂) angle of 129.69° is fairly close to the ideal value of 120°, which may explain the relatively high value of the binding energy. Similarly, a hydrogen-bond-like interaction C–H...O₁(CO₂) (the corresponding angle is 125.42°) and an electrostatic interaction between carbon of CO₂ and oxygen in the linker are also present.

Complexes D–G correspond to the CO₂ molecule being located above the oxamide group. A relatively strong binding has been found when the CO₂ molecule is located in a “bay” formed by a phenyl ring and the amide group (complex D, BE = –13.04 kJ mol⁻¹). Complex E (BE = –12.67 kJ mol⁻¹) highlights the importance of Coulombic interactions between carbon dioxide and the linker, in which the carbon of CO₂ is located directly above an oxygen of the linker, and an oxygen of CO₂ is found above the carbon of the linker. Complex F (BE = –10.25 kJ mol⁻¹) shows CO₂ positioned above the N–C bond, between the phenyl ring and an amide group. The least favourable binding site is found to be dimer G (BE = –7.61 kJ mol⁻¹) where the CO₂ molecule is located approxi-

mately midway between the carbons of the C–C bond between the two amide groups, but even this binding energy is stronger than that found for methane binding described above.

Finally, we compared the interactions of the CO₂ molecule with the oxamide part of the linker against those of CO₂ and solely the phenyl group (Figure 6), which has been replaced by a benzene ring. As this complex is somewhat smaller, more accurate calculations were undertaken in which both geometry optimisation and the BSSE-corrected binding energies were obtained directly at the MP2/cc-pvqz level of theory. Five stable configurations of the CO₂ molecule and benzene ring are

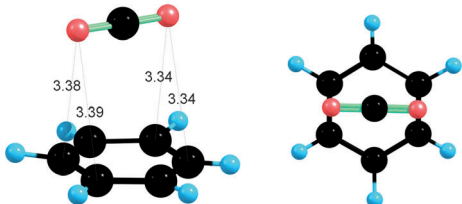
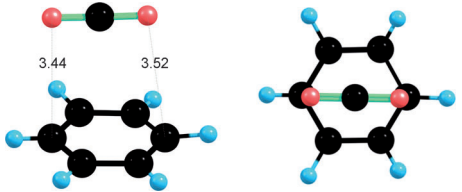
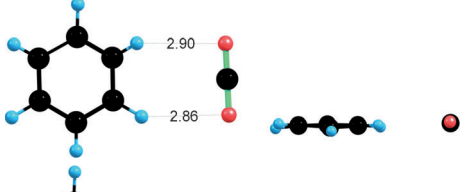
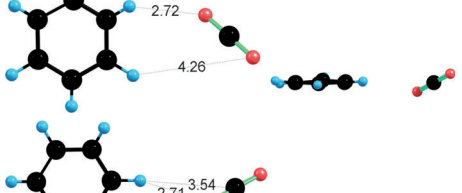
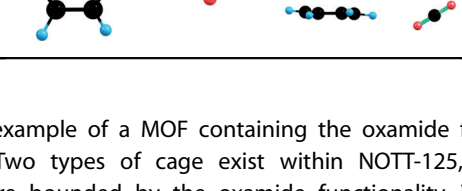
presented in Table 4. The strongest interaction corresponds to the cases in which the carbon atom of CO₂ is located directly above the middle of the benzene ring (complexes H and I). In the case of complex H (BE = –11.13 kJ mol⁻¹) the oxygen atoms of CO₂ are above the mid-points of two C–C bonds of the benzene ring, and the distances between the oxygen atoms of CO₂ and the nearest carbon atoms in the benzene ring are in the range of 3.34 to 3.39 Å. In complex I (BE = –10.54 kJ mol⁻¹), the oxygen atoms of CO₂ are above the carbon atoms of the benzene ring and the corresponding separation is slightly greater, being in the range 3.44 to 3.52 Å. The predicted values of the binding energies are in excellent agreement with previous calculations.^[30] The remaining three configurations (complexes J–L) are far less stable (BE in the range of –2 to –4 kJ mol⁻¹) and these correspond to the orientations in which CO₂ interacts side-on with the benzene ring.

Our calculations confirm that the oxamide part of the linker provides a variety of strong binding sites for CO₂ molecules with the values for the binding energy being significantly greater than those identified between CO₂ and the phenyl group, thus offering a clear preferential binding region in NOTT-125a. These binding modes are clearly not accessible in frameworks containing only single amides in their linkers. Additionally, in contrast to the CO₂–oxamide interactions, the binding identified between NOTT-125a and CH₄ is dependent on the presence of only one of the amide groups of the linker. The selectivity of NOTT-125a for CO₂ over CH₄, therefore, seems likely to be strongly influenced by the presence of this previously under-investigated oxamide motif.

Conclusion

In conclusion, we have successfully constructed a new highly porous **fof** type Cu^{II} paddlewheel porous material, the first re-

Table 4. The optimised MP2/cc-pvqz geometries and binding energies of C₆H₆-CO₂ complexes.

	Optimised geometry	Binding energy [kJmol ⁻¹]
H		-11.13
I		-10.93
J		-3.83
K		-3.06
L		-2.42

ported example of a MOF containing the oxamide functional group. Two types of cage exist within NOTT-125, both of which are bounded by the oxamide functionality. The large pore volume and functionalised pores are responsible for NOTT-125a exhibiting high CO₂ gas storage capacity and selectivity of CO₂ uptake over N₂ and CH₄. GCMC simulations of the gas uptake isotherms show excellent agreement with the experimental data, and our computational studies of the binding modes of CH₄ and CO₂ in NOTT-125a have identified a variety of strong binding sites for CO₂, which are only possible with the oxamide functionality.

Experimental Section

Commercially available reagents were used as received without further purification. Elemental analyses (C, H, and N) were performed on a CE-440 elemental analyser at the University of Nottingham. IR spectra were recorded in the range of 550–4000 cm⁻¹ on a Nicolet i5 FT-IR spectrophotometer using the attenuated total reflectance (ATR) mode. ¹H NMR spectra were recorded on a Bruker DPX-300 spectrometer. Thermal gravimetric analyses (TGA) were performed under a flow of nitrogen (20 mLmin⁻¹) with a heating rate of 1 °Cmin⁻¹ using a TA SDT-600 thermogravimetric analyser.

X-ray powder diffraction (PXRD) measurements were carried out at room temperature on a PANalytical X'Pert PRO diffractometer using Cu_{Kα1} radiation (λ = 1.5418 Å) at 40 kV, 40 mA, at a scan-speed of 0.02 °s⁻¹ and a step size of 0.005° in 2θ.

N₂, H₂ and CO₂ isotherms

N₂, H₂ and CO₂ isotherms were determined using an IGA gravimetric adsorption apparatus (Hidden) at the University of Nottingham in a clean ultra-high vacuum system with a diaphragm and turbo pumping system. Before measurements, about 120 mg of solvent-exchanged sample was loaded into the sample basket within the adsorption instrument and then degassed under dynamic vacuum at 100 °C for 16 h to obtain the fully desolvated samples.

Synthesis of H₄L

A solution of 5-aminoisophthalic acid (6.53 g, 34.2 mmol) in anhydrous THF (50 mL) was cooled at 0 °C. A solution of oxalyl chloride (1.0 mL, 11.4 mmol) in anhydrous THF (100 mL) was then added dropwise to the reaction mixture over a period of 1 h and a precipitate was formed almost immediately. Triethylamine (1.0 mL, 7.2 mmol) was slowly added after 1 h and the mixture was stirred overnight (~12 h) at room temperature. The volume of solvent was partially reduced in the rotary evaporator and then 2 M HCl (200 mL) was added to the mixture. The precipitate was isolated by filtration and washed extensively with water, recrystallised from methanol, filtered, washed with methanol and diethyl ether, and dried under vacuum to afford a white powder (2.47 g, 58% yield). ¹H NMR (300 MHz, [D₆]DMSO): δ = 13.08 (s, 4H, COOH), 11.26 (s, 2H, NH), 8.72 (d, J = 1.2 Hz, 4H, Ar-H), 8.26 ppm (t, J = 1.2 Hz, 2H, Ar-H); ¹³C NMR (75 MHz, [D₆]DMSO): δ = 166.81, 159.24, 138.80, 132.30, 126.43, 125.68 ppm; ATR FT-IR: ν̄ = 3227 (m), 2158 (w), 1974 (w), 1716(s), 1681(s), 1653(s), 1558 (m), 1540 (s), 1456 (m), 1387 (s), 1301(m), 1275 (s), 1185 (w), 952 (m), 841(m), 758 (s), 728 (s), 670 cm⁻¹ (m); HRMS (EI-): m/z 439.0403 [M+Na]⁺, 434.0838 [M+H₄N]⁺, 415.0401 [M-H]⁻; elemental analysis calcd (%) for C₁₈H₈N₂O₁₀: C 51.93, H 2.98, N 6.73; found: C 51.47, H 3.05, N 6.56.

Synthesis of NOTT-125, [Cu₂(C₁₈H₁₂O₁₀N₂)(H₂O)₂]-2DMA-4H₂O

H₄L (0.03 g, 0.081 mmol) and Cu(NO₃)₂·3H₂O (0.06 g, 0.516 mmol) were added to a DMA/H₂O solvent (9:2, 5.5 mL). HBF₄ (50% in H₂O, 0.2 mL) was added and the solution was thoroughly mixed. The solution was heated without stirring at 70 °C using an oil-bath for 48 h and a large amount of microcrystalline product precipitated. The blue crystalline product was separated by filtration, washed with warm DMA and dried briefly in air. Yield: 0.15 g (60%); elemental analysis calcd (%) for C₂₆H₃₈Cu₂N₄O₁₈: C 38.00, H 4.60, N 6.82; found: C 39.10, H 4.82, N 6.85.

The Supporting Information includes additional views of the crystal structures, TGA and PSD analysis, PXRD, technical details for gas adsorption experiments and gas isotherms.

CCDC-965874 (NOTT-125) contains the supplementary crystallographic data for this paper. These data can be obtained free of charge from The Cambridge Crystallographic Data Centre via www.ccdc.cam.ac.uk/data_request/cif.

Acknowledgements

We thank the EPSRC and the University of Nottingham for support and funding. M.S. gratefully acknowledges receipt of an ERC Advanced Grant, and E.B. an ERC Starter Grant. N.H.A. thanks the Royal Commission for Jubail and Yanbu, Jubail University College, Kingdom of Saudi Arabia for a PhD Fellowship, C.P.K. thanks Conacyt, Mexico for funding, and J.L. thanks the Royal Society for a Sino–British Fellowship.

Keywords: carboxylic acid · CO₂ · copper · isophthalate · metal–organic frameworks

- [1] a) H. Furukawa, N. Ko, Y. B. Go, N. Aratani, S. B. Choi, E. Choi, A. Ö. Yazaydin, R. Q. Snurr, M. O’Keeffe, J. Kim, O. M. Yaghi, *Science* **2010**, *329*, 424–428; b) O. K. Farha, A. Ö. Yazaydin, I. Eryazici, C. D. Malliakas, B. G. Hauser, M. G. Kanatzidis, S. T. Nguyen, R. Q. Snurr, J. T. Hupp, *Nat. Chem.* **2010**, *2*, 944–948; c) J.-R. Li, J. Sculley, H.-C. Zhou, *Chem. Rev.* **2012**, *112*, 869–932; d) K. Koh, A. G. Wong-Foy, A. J. Matzger, *J. Am. Chem. Soc.* **2009**, *131*, 4184–4185; e) S. Yang, X. Lin, A. J. Blake, G. S. Walker, P. Hubberstey, N. R. Champness, M. Schröder, *Nat. Chem.* **2009**, *1*, 487–493; f) X. Lin, J. Jia, X. B. Zhao, K. M. Thomas, A. J. Blake, N. R. Champness, P. Hubberstey, M. Schröder, *Angew. Chem.* **2006**, *118*, 7518–7524; *Angew. Chem. Int. Ed.* **2006**, *45*, 7358–7364; g) X. Lin, J. Jia, P. Hubberstey, M. Schröder, N. R. Champness, *CrystEngComm* **2007**, *9*, 438–448.
- [2] a) J. Liu, P. K. Thallapally, B. P. McGrail, D. R. Brown, J. Liu, *Chem. Soc. Rev.* **2012**, *41*, 2308–2322; b) D. M. D’Alessandro, B. Smit, J. R. Long, *Angew. Chem.* **2010**, *122*, 6194–6219; *Angew. Chem. Int. Ed.* **2010**, *49*, 6058–6082; c) A. R. Millward, O. M. Yaghi, *J. Am. Chem. Soc.* **2005**, *127*, 17998–17999.
- [3] a) Z. Zhang, Y. Zhao, Q. Gong, Z. Li, J. Li, *Chem. Commun.* **2013**, *49*, 653–661; b) J.-R. Li, Y. Ma, M. C. McCarthy, J. Sculley, J. Yu, H.-K. Jeong, B. Balbuena, H.-C. Zhou, *Coord. Chem. Rev.* **2011**, *255*, 1791–1823; c) K. Sumida, D. L. Rogow, J. A. Mason, T. M. McDonald, E. D. Bloch, Z. R. Herm, T.-H. Bae, J. R. Long, *Chem. Rev.* **2012**, *112*, 724–781.
- [4] a) W. Yang, A. J. Davies, X. Lin, M. Suyetin, R. Matsuda, A. J. Blake, C. Wilson, W. Lewis, J. E. Parker, C. C. Tang, M. W. George, P. Hubberstey, S. Kitagawa, H. Sakamoto, E. Bichoutskaia, N. R. Champness, S. Yang, M. Schröder, *Chem. Sci.* **2012**, *3*, 2993–2999; b) S. Yang, X. Lin, W. Lewis, M. Suyetin, E. Bichoutskaia, J. Parker, C. C. Tang, D. R. Allan, P. J. Rizkallah, P. Hubberstey, N. R. Champness, K. M. Thomas, A. J. Blake, M. Schröder, *Nat. Mater.* **2012**, *11*, 710–716; c) S. Yang, J. Sun, A. J. Ramirez-Cuesta, S. K. Callear, W. I. F. David, D. Anderson, R. Newby, A. J. Blake, J. E. Parker, C. C. Tang, M. Schröder, *Nat. Chem.* **2012**, *4*, 887–894.
- [5] a) L. J. Murray, M. Dincă, J. R. Long, *Chem. Soc. Rev.* **2009**, *38*, 1294–1314; b) H. Furukawa, M. A. Miller, O. M. Yaghi, *J. Mater. Chem.* **2007**, *17*, 3197–3204.
- [6] X. Lin, N. R. Champness, M. Schröder, *Top. Curr. Chem.* **2010**, *293*, 35–76.
- [7] Y. Zhao, H. Wu, T. J. Emge, Q. Gong, N. Nijem, Y. J. Chabal, L. Kong, D. C. Langreth, H. Liu, H. Zeng, J. Li, *Chem. Eur. J.* **2011**, *17*, 5101–5109.
- [8] X. Si, C. Jiao, F. Li, J. Zhang, S. Wang, S. Liu, Z. Li, L. Sun, F. Xu, Z. Gabelica, C. Schick, *Energy Environ. Sci.* **2011**, *4*, 4522–4527.
- [9] C. Zlotea, D. Phanon, M. Mazaj, D. Heurtaux, V. Guillermin, C. Serre, P. Horcajada, T. Devic, E. Magnier, F. Cuevas, G. Férey, P. L. Llewellyn, M. Latroche, *Dalton Trans.* **2011**, *40*, 4879–4881.
- [10] A. Demessence, D. M. D’Alessandro, M. L. Foo, J. R. Long, *J. Am. Chem. Soc.* **2009**, *131*, 8784–8786.
- [11] a) R. Vaidhyanathan, S. S. Iremonger, K. W. Dawson, G. K. H. Shimizu, *Chem. Commun.* **2009**, 5230–5232; b) S. Couck, J. F. M. Denayer, G. V. Baron, T. Remy, J. Gascon, F. Kapteijn, *J. Am. Chem. Soc.* **2009**, *131*, 6326–6327.
- [12] F. Debatin, A. Thomas, A. Kelling, U. Hedin, Z. Bacsik, I. Senkovska, S. Kaskel, M. Junginger, H. Müller, U. Schilde, C. Jager, A. Friedrich, H.-J. Holdt, *Angew. Chem.* **2010**, *122*, 1280–1284; *Angew. Chem. Int. Ed.* **2010**, *49*, 1258–1262.
- [13] J. An, S. J. Geib, N. L. Rosi, *J. Am. Chem. Soc.* **2010**, *132*, 38–39.
- [14] B. Arstad, H. Fjellvåg, K. Kongshaug, O. Swang, R. Blom, *Adsorption* **2008**, *14*, 755–762.
- [15] Y. Yan, M. Suyetin, E. Bichoutskaia, A. J. Blake, D. R. Allan, S. A. Barnett, M. Schröder, *Chem. Sci.* **2013**, *4*, 1731–1736.
- [16] a) B. Zheng, J. Bai, J. Duan, L. Wojtas, M. J. Zaworotko, *J. Am. Chem. Soc.* **2011**, *133*, 748–751; b) D. Q. Yuan, D. Zhao, D. F. Sun, H.-C. Zhou, *Angew. Chem.* **2010**, *122*, 5485–5489; *Angew. Chem. Int. Ed.* **2010**, *49*, 5357–5361.
- [17] B. Chen, S. Xiang, G. Qian, *Acc. Chem. Res.* **2010**, *43*, 1115–1124.
- [18] P. D. C. Dietzel, V. Besikiotis, R. Blom, *J. Mater. Chem.* **2009**, *19*, 7362–7370.
- [19] M. Dincă, J. R. Long, *Angew. Chem.* **2008**, *120*, 6870–6884; *Angew. Chem. Int. Ed.* **2008**, *47*, 6766–6779.
- [20] a) X. Lin, I. Telepeni, A. J. Blake, A. Dailly, C. Brown, J. Simmons, M. Zoppi, G. S. Walker, K. M. Thomas, T. J. Mays, P. Hubberstey, N. R. Champness, M. Schröder, *J. Am. Chem. Soc.* **2009**, *131*, 2159–2171; b) Y. Yan, X. Lin, S. Yang, A. J. Blake, A. Dailly, N. R. Champness, P. Hubberstey, M. Schröder, *Chem. Commun.* **2009**, 1025–1027; c) Y. Yan, I. Telepeni, S. Yang, X. Lin, W. Kockelmann, A. Dailly, A. J. Blake, W. Lewis, G. S. Walker, D. R. Allan, S. A. Barnett, N. R. Champness, M. Schröder, *J. Am. Chem. Soc.* **2010**, *132*, 4092–4094; d) Y. Yan, A. J. Blake, W. Lewis, S. A. Barnett, A. Dailly, N. R. Champness, M. Schröder, *Chem. Eur. J.* **2011**, *17*, 11162–11170.
- [21] Y. Yan, S. Yang, A. J. Blake, W. Lewis, E. Poirier, S. A. Barnett, N. R. Champness, M. Schröder, *Chem. Commun.* **2011**, *47*, 9995–9997.
- [22] a) M. O’Keeffe, O. Yaghi, *Chem. Rev.* **2012**, *112*, 675–702; b) Z. Wang, B. Zheng, H. Liu, X. Lin, X. Yu, P. Yi, R. Yun, *Cryst. Growth Des.* **2013**, *13*, 5001–5006.
- [23] A. L. Spek, PLATON, *Acta Crystallogr. Sect. D* **2009**, *65*, 148–155.
- [24] J. Park, J.-R. Li, Y.-P. Chen, J. Yu, A. A. Yakovenko, Z. U. Wang, L.-B. Sun, P. B. Balbuena, H.-C. Zhou, *Chem. Commun.* **2012**, *48*, 9995–9997.
- [25] a) B. Li, Z. Zhang, Y. Li, K. Yao, Y. Zhu, Z. Deng, F. Yang, X. Zhou, G. Li, H. Wu, N. Nijem, Y. J. Chabal, Z. Lai, Y. Han, Z. Shi, S. Feng, J. Li, *Angew. Chem.* **2012**, *124*, 1441–1444; *Angew. Chem. Int. Ed.* **2012**, *51*, 1412–1415; b) R. Luebke, J. F. Eubank, A. J. Cairns, Y. Belmabkhout, L. Wojtas, M. Eddaoudi, *Chem. Commun.* **2012**, *48*, 1455–1457.
- [26] a) B. Zheng, H. Liu, Z. Wang, X. Yu, P. Yi, J. Bai, *CrystEngComm* **2013**, *15*, 3517–3520; b) B. Zheng, Z. Yang, J. Bai, Y. Li, S. Li, *Chem. Commun.* **2012**, *48*, 7025–7027; c) J. Duan, Z. Yang, J. Bai, B. Zheng, Y. Li, S. Li, *Chem. Commun.* **2012**, *48*, 3058–3060; d) Z. Lu, H. Xing, R. Sun, J. Bai, B. Zheng, Y. Li, *Cryst. Growth Des.* **2012**, *12*, 1081–1084.
- [27] M. S. Sun, D. B. Shah, H. H. Xu, O. Talu, *J. Phys. Chem. B* **1998**, *102*, 1466–1473.
- [28] Y. Shao, L. F. Molnar, Y. Jung, J. Kussmann, C. Ochsenfeld, S. T. Brown, A. T. B. Gilbert, L. V. Slipchenko, S. V. Levchenko, D. P. O’Neill, R. A. DiStasio, R. C. Lochan, T. Wang, G. J. O. Beran, N. A. Besley, J. M. Herbert, C. Y. Lin, T. Van Voorhis, S. H. Chien, A. Sodt, R. P. Steele, V. A. Rassolov, P. E. Maslen, P. P. Korambath, R. D. Adamson, B. Austin, J. Baker, E. F. C. Byrd, H. Dachsel, R. J. Doerksen, A. Dreuw, B. D. Dunietz, A. D. Dutoi, T. R. Furlani, S. R. Gwaltney, A. Heyden, S. Hirata, C. P. Hsu, G. Kedziora, R. Z. Khallilulin, P. Klunzinger, A. M. Lee, M. S. Lee, W. Liang, I. Lotan, N. Nair, B. Peters, E. I. Proynov, P. A. Pieniazek, Y. M. Rhee, J. Ritchie, E. Rosta, C. D. Sherrill, A. C. Simmonett, J. E. Subotnik, H. L. Woodcock, W. Zhang, A. T. Bell, A. K. Chakraborty, D. M. Chipman, F. J. Keil, A. Warshel, W. J. Hehre, H. F. Schaefer, J. Kong, A. Krylov, P. M. W. Gill, M. Head-Gordon, *Phys. Chem. Chem. Phys.* **2006**, *8*, 3172–3191.
- [29] a) G. R. Desiraju, T. Steiner, *The Weak Hydrogen Bond in Structural Chemistry and Biology*, Oxford University Press, **1999**; b) G. R. Desiraju, *Acc. Chem. Res.* **1991**, *24*, 290–296; c) S. Varughese, S. M. Drapper, *Cryst. Growth Des.* **2010**, *10*, 2298–2305.
- [30] S. S. Han, D. Kim, D. H. Jung, S. Cho, S.-H. Choi, Y. J. Jung, *J. Phys. Chem. C* **2012**, *116*, 20254–20261.

Received: October 14, 2013

Revised: January 12, 2014

Published online on May 7, 2014